PERGAMON

Vision Research 40 (2000) 1955–1967

Vision Research

www.elsevier.com/locate/visres

Representation of stereoscopic edges in monkey visual cortex

Rüdiger von der Heydt [a,b,*], Hong Zhou [a], Howard S. Friedman [a,c]

[a] *Krieger Mind/Brain Institute, 3400 North Charles Street, Johns Hopkins University, Baltimore, MD 21218, USA*
[b] *Department of Neuroscience, 3400 North Charles Street, Johns Hopkins University, Baltimore, MD 21218, USA*
[c] *Department of Biomedical Engineering, 3400 North Charles Street, Johns Hopkins University, Baltimore, MD 21218, USA*

Received 25 January 1999; received in revised form 15 October 1999

Abstract

Form perception in random-dot stereograms is based on information that resides in the correlation between the two images, but is not present in either image alone. We have studied the coding of stereoscopic figures in the neural activity of areas V1 and V2 of alert behaving monkeys. While cells in V1 generally responded according to the disparity of the surface at the receptive field, we found cells in area V2 that responded selectively to the figure edges. These cells signaled the location and orientation of contrast borders as well as stereoscopic edges, and were often selective for the direction of the step in depth. We concluded that stereoscopic edges are explicitly represented in area V2. © 2000 Elsevier Science Ltd. All rights reserved.

Keywords: Three-dimensional form perception; Stereopsis; Single neuron; Visual cortex

1. Introduction

One of the amazing features of visual perception is the ability to utilize minute mismatches in the images of the two eyes for stereopsis. Using computer-generated random-dot stereograms Bela Julesz discovered that stereopsis does not require the presence of recognizable features in the two images (Julesz, 1960). Viewing such a stereogram binocularly reveals the clear shape of a figure (a floating diamond in the example of Fig. 1B), although only random dots are presented to both eyes. Thus, one can perceive binocularly objects which are monocularly invisible. This phenomenon has been called cyclopean perception, alluding to Helmholtz' cyclopean eye, the hypothetical representation that combines the views of the two eyes (Julesz, 1971). Several neurophysiological studies have identified binocular cells in the visual cortex that are sensitive to spatial mismatches (disparities) in the two images (Barlow, Blakemore & Pettigrew, 1967; Nikara, Bishop & Pettigrew, 1968; Hubel & Wiesel, 1970; Poggio & Fischer, 1977; Hubel & Livingstone, 1987; see Poggio, 1995, for a review of the results in monkey). While these cells provide local depth information, it is not clear whether they would detect the contours of a figure in a random-dot stereogram such as Fig. 1B. Hence the neural basis of binocular shape perception has remained elusive. We have studied the activity of cells in areas V1 and V2 of the monkey visual cortex in order to determine if there is an explicit contour representation for binocular shape perception. Specifically, we have asked whether the neural signals represent position and orientation of cyclopean edges, and whether the signals carry information about the direction of foreground and background, which is essential for 3D form perception. Preliminary results have been published in abstract form (von der Heydt, Zhou & Friedman, 1995).

2. Materials and methods

Monkeys (*Macaca mulatta*) were prepared for recording by attaching a peg for head fixation and two recording chambers (over left and right visual cortex) to the skull with bone cement and surgical screws. The surgery was done under aseptic conditions in pentobarbital anesthesia. Anesthesia was induced with ketamine, and buprenorphine was used for postoperative analgesia. Other details of our methods are described in von

* Corresponding author. Tel.: +1-410-5166416; fax: +1-410-5168648.
E-mail address: von.der.heydt@jhu.edu (R. von der Heydt)

PII: S0042-6989(00)00044-4

der Heydt and Peterhans (1989). All procedures conformed to the principles regarding the care and use of animals adopted by the American Physiological Society and the Society for Neuroscience, as verified by the Animal Care and Use Committee of the Johns Hopkins University.

2.1. Recording

Several weeks after the surgery, 1–2 days before the beginning of recording, a 3 mm trephination was made in one of the chambers under ketamine anesthesia. On each day of recording, granulation tissue was removed from the dura, the hole was sealed with bone wax, and a micro-electrode for extracellular recording was inserted through the wax and the dura mater, using a microdrive and positioning device mounted on the chamber. Electrode and wax were removed after the session, and dexamethasone drops were applied to reduce tissue reaction. After a few days of recording, the dura was carefully thinned under a dissection microscope. Good recordings with minimal dimpling of cortex were usually possible for 2–3 weeks after drilling a hole. After a break of 1 week or more, another hole was drilled and recording resumed, for up to five holes in each chamber. Electrodes with fine tips were used that easily isolated single units, but also picked up some background activity (PtIr 0.1 mm. diameter, taper 0.07–0.1, glass-coated, impedance 3–10 MΩ at 1 kHz). These electrodes isolated about 22 cells on average in vertical penetrations through V1 and also picked up action potentials of fibers in the white matter. While advancing the electrode, we carefully monitored the entry into the cortex, the amount of single- and multi-unit activity, its orientation and ocularity preference, the entry into the white matter, the entry into the cortex below the white matter, etc. The corresponding depths were recorded graphically. Comparison of many such *track charts* (about 50 per hemisphere) with the histological reconstructions has shown that layers 4B, 4C and 6 in V1 can often be identified physiologically during the recording (von der Heydt & Peterhans, 1989). Cells were recorded in the central visual field representations of areas V1 (0.4–6.0°, median 3.2°) and V2 (0.2–8.6°, median 3.5°) of two animals.

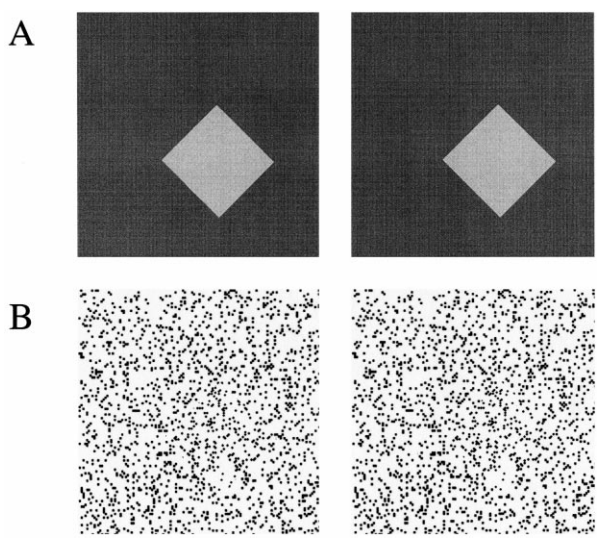

Fig. 1. Examples of the stereograms used in this study. (A) Contrast-defined figure. (B) Random-dot stereogram, in which the figure can only be perceived binocularly, that is, when the two half-images are viewed separately by left and right eyes ('cyclopean figure'). In (A) the diamonds are slightly displaced horizontally between left and right images, as are the corresponding regions of dot patterns in (B), causing the binocular perception of a figure floating in depth. In the experiments, a pair of fixation targets was also presented.

2.2. Anatomical methods

The recording sites were verified by histological reconstruction. After the recordings were completed, the animal was anesthetized, and thin (0.25 mm), sharply pointed marker pins were inserted in parallel tracks at known positions around the recording regions using the same positioning device that was used for recording. The animal was then killed with an overdose of pentobarbital and the brain perfused through the heart with saline followed by buffered 4% formaldehyde. The pins were then removed, the tissue was blocked and soaked in 30% sucrose, and 50 μ frozen sections were cut at right angles to the orientation of the pins (tangential sections). The sections were stained for cytochrome oxidase. Outlines, layers, and pin holes were traced using a computer controlled microscope (Neurolucida). These tracings were plotted together with the positions of the recording tracks (in principle, the tracks in each hemisphere were all parallel to the marker pins). The positions of the recording tracks were calculated from the electrode positioning coordinates using an alignment transformation (rotation, shift, and scaling in the tangential plane). The transformation matrix was obtained by performing a least squares fit between the coordinates of pin insertion, as read from the positioning device, and the measured locations of the pinholes in the tissue. The depths of the recorded cells were determined by aligning the depth records in our track charts with the corresponding anatomical landmarks.

2.3. Visual stimulation

The animal performed a fixation task by looking through a mirror stereoscope at a CRT display. Pairs of fixation targets and test stimuli were generated side-by-side on a computer monitor (Hitachi HM4119) with a 60 Hz refresh rate. The display (resolution 1280 × 1024 pixels) was generated by an Omnicomp GDS 2000 processor controlled by a PC. The field of stimulation

measured 11.5° square for each eye, with a resolution of 400×400 pixels. Contrast-defined figures had a luminance between 1.3 and 67 cd/m^2 (depending on figure color) and were presented on a background of 20 cd/m^2 neutral gray. The random-dot stereograms (Julesz, 1971) consisted of 5 arc min dots of 25 cd/m^2 on a background of 15 cd/m^2, with 10%, sometimes 50%, dot density. For cells that were color selective, colored dots were used. The results presented below were obtained mainly with static stimuli, but dynamic random-dot stereograms were also used (pattern renewal at 60 Hz). Flashing and moving bars were used for the preliminary assessment of receptive field properties.

2.4. Fixation training

The animals were trained to fixate their gaze by requiring them to respond to an orientation change that could only be resolved in foveal vision. The fixation target was a small white square divided by a gray line whose change from vertical to horizontal had to be detected. The target was centered on a 19 arc min black square with the purpose to facilitate fixation when the target was presented on a random-dot pattern. The general trial sequence was as follows: Target onset, monkey responds by pulling a lever and begins to fixate, 0.5–5 s variable interval (fixation period), target rotates, monkey responds by releasing lever, 1–2 s variable interval (monkey usually looks away from target), new trial begins with target onset, etc. Eye movement control with a fixation window was used during the training to improve the reliability of fixation. Eye movements were recorded monocularly using a TV-based infrared pupil tracking system (Iscan). The size of the fixation target was gradually lowered to 7 arc min, the width of the line to be discriminated to 1.7 arc min, and the limit for the response time to 400 ms. The contrast of the dividing line was then adjusted for each monkey until fixation became steady, as indicated by a low frequency of fixation breaks detected by the eye movement monitor. Training was continued until the animals performed the task reliably for several hours. The hit rate during recording sessions was about 95% on average. Although the eye movement recording was only monocular, we believe that the task difficulty also enforced accurate binocular convergence. This was evident from the disparity tunings of many neurons in which disparity differences of 3 arc min reliably produced large response changes (see example in Fig. 9).

2.5. Procedure

Upon isolating a cell, the 'minimum response field' was determined. This is defined as the visual field region that an optimally configured bar stimulus must enter in order to evoke a response (Barlow et al., 1967). We used stereoscopically presented contrast bars that were optimized for length and width, orientation, color and disparity. Orientation and disparity tuning were assessed with moving bars, in most cases by recording complete tuning curves, including monocular controls. The disparity tuning was classified as 'tuned excitatory', 'near', 'far', 'tuned inhibitory', or 'flat' using the qualitative criteria of Poggio and Fischer (1977). Specifically, 'near' and 'far' cells were distinguished by their asymmetric tuning curves with a steep slope near zero disparity, as compared to 'tuned' cells which showed symmetrical tuning. In order to record a representative sample, an exhaustive analysis was attempted. In other words, we did not skip 'difficult' cells. It often took us considerable time to find the appropriate stimulus if cells were selective for several stimulus parameters. After this preliminary assessment we tested contrast-defined and cyclopean figures (see Fig. 1). These were squares of 4° size (occasionally 6°), which were presented with the preferred edge orientation and disparity. The disparity of the 11.5° surround could also be varied relative to the fixation target. This disparity was set either to zero (the distance of fixation) or to a 'far' value, depending on the disparity of the figure, so that the figure appeared to float in front of the surround. The 4° size was large compared to the typical response fields of near-foveal cells of V1 and V2. Position response profiles were obtained by varying figure position orthogonal to the optimal orientation. Sixteen positions (spaced 0.5°) were presented in pseudo-random order, and additional positions were tested occasionally. Edge orientation was varied by rotating the figure about one edge that was centered in the receptive field, and 16 orientations covering 360° were tested. The figures were stationary except for the position and orientation changes which occurred between the fixation periods. The random-dot patterns were generally static, with a new pattern generated for each fixation period. The major findings of cyclopean edge selectivity and orientation tuning were also confirmed with dynamic random-dot stereograms.

2.6. Data analysis

Only well isolated single cell activity was analyzed. Spike events were digitized online and the activity during fixation periods was analyzed, beginning 300 ms after the monkey's response to target onset and ending at the moment of target rotation (see Fig. 3). The 300 ms delay was used to allow fixation to settle. Average numbers of spikes per second were determined for a total of at least 4 s for each stimulus condition, which were in general distributed over several fixation periods. The peaks of the position response profiles and orientation tuning curves were defined as the midpoints at half height of the smoothed response curves (2-point run-

ning average). Edge selectivity was quantified by the surface to edge response ratio (SER) which was defined as $(R_{inside} - R_{outside})/(R_{edge} - R_{outside})$, where R_{inside} and $R_{outside}$ are the mean numbers of spikes for positions near the center ($\pm 0.5°$) and outside the figure ($\geq 1°$ distance from edge), respectively, and R_{edge} is the maximum of the mean numbers of spikes for positions near the edges of the figure ($\pm 0.5°$). In cases where 6° rather than 4° squares were used, these ranges were scaled correspondingly.

3. Results

Binocular disparity selectivity was studied for 334 cells in two monkeys, 172 of V1, and 162 of V2. In V1, 89% of our data come from layer 2/3. In both areas, the vast majority of cells were sensitive to binocular disparity when tested with moving contrast bars; in 72% of the cells the response to the best disparity was at least three times stronger than the response to the worst disparity (V1: 65%, V2: 78%). 'Tuned-excitatory', 'near', 'far' and 'tuned-inhibitory' cells were found (Poggio & Fischer, 1977; Poggio, 1995), with frequencies of 34, 10, 12 and 8%, respectively in V1, and 37, 25, 12 and 4% in V2, plus three cells with bimodal tuning (two in V1 and one in V2).

A total of 144 cells were studied with cyclopean figures, 69 in V1, and 75 in V2. The selection was mainly determined by our ability to hold stable recording long enough and by the working hours of the monkeys. The proportion of disparity sensitive cells in this sample was 74%, virtually the same as that of the larger sample. The recording sites of the cells tested with cyclopean figures were spread over large portions of V1 and V2, and the receptive field eccentricities were comparable in the two areas: 1.4–6.0° (median 3.3°) for V1, and 0.9–6.9° (median 3.7°) for V2. In animal #1, 128 cells (65 of V1, 63 of V2) were studied with cyclopean figures in 73 penetrations in two hemispheres; in animal #2, 16 cells (four of V1, 12 of V2) were studied in 15 penetrations in one hemisphere. The cells were tested with cyclopean figures centered about the receptive field, and with edges of such figures at the preferred orientation. We first set the figure disparity to the preferred value (as determined with contrast bars) and the surround disparity to zero, or to a positive (far) value, typically seven or 14 arc min, if the cell's preferred disparity was close to zero or positive. If a cell did not respond well with these disparities, other combinations were explored. Of the 144 cells tested, 81 (57%) responded weakly or not at all to the random-dot stereograms (although all of them responded well to contrast stimuli). Most of these cells were completely silenced or responded with less than 2 spikes/s. In every case, unresponsiveness was assessed for the center of the figure as well as for the edges, and by varying figure and surround disparities. Disparity selectivity was about as common among cells that were activated by random-dot stereograms as among cells that were not activated (84 vs 73%, n.s.). Thus, whether or not a cell could be activated by a random-dot stereogram was not related to its disparity selectivity.

Position response profiles for cyclopean figures were completed in 104 cells, 63 of which (27 of V1, 36 of V2) were sufficiently activated for the profiles to be analyzed quantitatively.

3.1. Edge selectivity

Fig. 2 represents the responses of four cells, one of V1, and three of V2, to contrast-defined figures (as shown in Fig. 1A), and to monocularly invisible, cyclopean figures (as shown in Fig. 1B). Previous tests with moving contrast bars had revealed that all of these cells were orientation and disparity selective. In this experiment, stationary 4° squares of optimal orientation and disparity were presented at 16 different positions in the visual field. The inset at the bottom of Fig. 2 shows the position variation schematically, as if the receptive fields (small rectangles) had scanned the figures (large squares). The positions marked by dots correspond to the data points above, that is, for $-2°$, the receptive field was centered on the left edge of the figure, for 0°, in the middle, for 2°, on the right edge, etc.

With the contrast-defined figure, all four cells responded only when the receptive field was positioned on an edge (top row). However, with the cyclopean figure, cell 1 was activated whenever the receptive field entered the figure, whereas cells 2–4 were again activated only on the edges, just as with the contrast-defined figure. The behavior of cell 1 would be expected in disparity selective cells, as known from previous studies (Poggio & Fischer, 1977; Poggio, Motter, Squatrito & Trotter, 1985). The cell was activated over the area of the cyclopean figure (where the disparity of the dot patterns was optimal), but the figure edges did not produce any stronger response. The new finding is the behavior of cells 2–4, which responded to edges but not the surface of the cyclopean figure. Fig. 3 shows event plots of the responses of cells 1 and 2 to the cyclopean-figure stereograms. The times of action potentials are plotted relative to the moment of lever pulling (which generally indicates the beginning of fixation), and the responses are arranged according to stimulus position, as indicated on the left. Responses to repeated presentations have been offset vertically for clarity. One can see the elevated activity of cell 1 for receptive field positions within the figure boundaries (dashed lines) and the strong, selective activation of cell 2 for positions near the figure edges. Note that a new random-

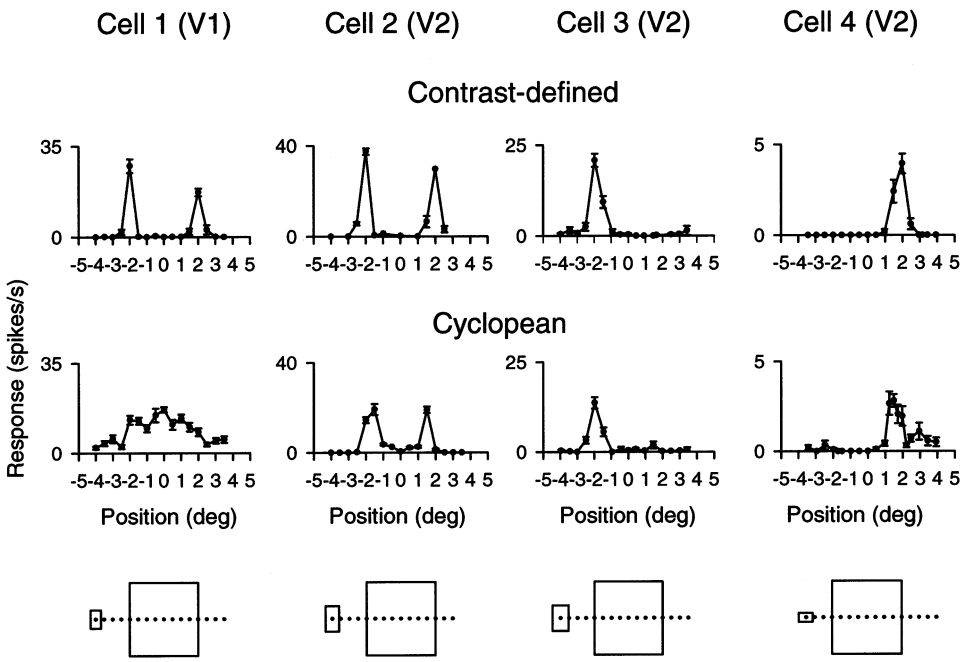

Fig. 2. Neural responses to contrast-defined and cyclopean figures. Static figures were presented at different positions relative to the cells' receptive fields. The positional relationship is shown schematically at the bottom, as if the receptive fields had scanned the figures. The small rectangles represent minimum response fields, the large squares represent test figures. Data points in the graphs correspond to the dotted positions below. Position-response functions like these, obtained from single cells, can be read as activity profiles across families of similar cells with receptive fields distributed across the figure. The above response functions show that the family of cell 1 represents edges for contrast-defined figures, but surface for cyclopean figures, whereas the families of cells 2–4 represent edges for both types of figures. All four cells were tuned to disparity. Cell 1: layer 2/3 of area V1, cells 2–4, area V2. The disparities of figure/surround were $-14'/0'$, $+4'/+28'$, $-9'/0'$, $-10'/0'$, respectively (positive = far, negative = near), the orientations were 136, 120, 90 and 80°. Stimuli and receptive fields are drawn with 90° orientation instead to facilitate comparison.

dot pattern was presented for each trial. Thus, some of the trial-to-trial variation of responses is due to the variation of the pattern. A somewhat irregular activity, as seen in the plot of cell 1, was typical for cells of V1. It might be due to the small receptive field size of these cells which makes them sensitive to displacements of the retinal stimulus caused by residual eye movements.

To quantify cyclopean edge selectivity we calculated the ratio of surface and edge response strengths (SER, see Section 2.6) for the 63 cells that gave sufficient responses. Eight of these (three of V1 and five of V2) had position response profiles that were flat or not obviously related to figure surface or edges and thus would not give meaningful ratios. These were excluded as 'unclear'. The resulting distributions of the SER for V1 and V2 are shown in Fig. 4. It can be seen that ratios near zero and negative ratios were common in cells of V2. These cells responded to one or both edges of the figure, but not the center (a negative ratio means that the activity was lower for the center of the figure than outside the figure). Cells of this kind were not found in V1, although some V1 cells had ratios well below 1, indicating edge enhancement. A few cells in both areas showed ratios of 1 or greater, indicating that the responses to the edges were equal or weaker than

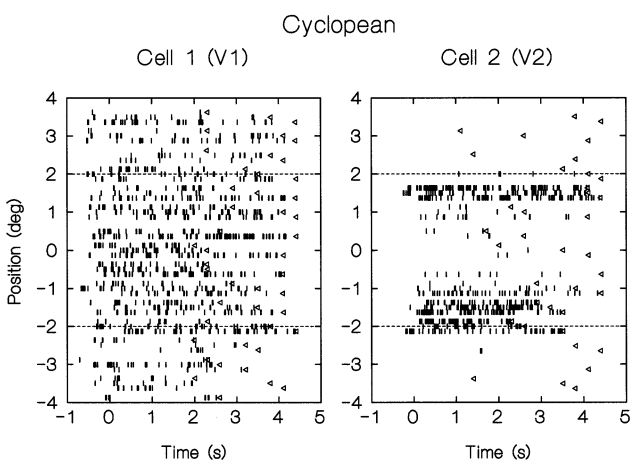

Fig. 3. Event plots of the responses of cells 1 and 2 to the cyclopean-figure stereograms. Small vertical lines represent action potentials, the abscissa indicates the time after the animal initiated a trial by pulling a lever (the beginning of fixation), triangles indicate the time of rotation of the fixation target to which the animal had to respond (the end of fixation). The ordinate represents receptive field position relative to the figure. Up to 3 trials are represented for each position, with small vertical offsets. One can see the increased activity of cell 1 for receptive field positions within the figure boundaries (dashed lines), and the selective activation of cell 2 for positions near the figure edges.

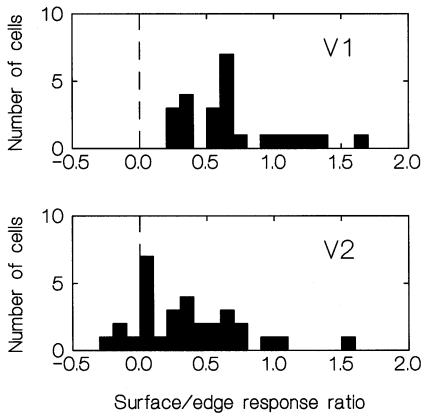

Fig. 4. The distribution of the ratio of surface response to edge response in cells of cortical areas V1 ($n = 24$) and V2 ($n = 36$). See Section 2.6 for definition of ratio.

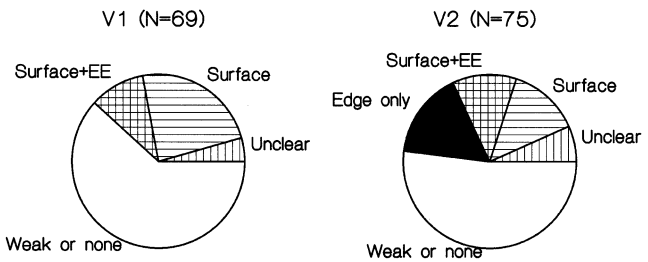

Fig. 5. Summary of the types of responses to random-dot stereograms encountered in cortical areas Vl and V2. Cells were classified according to their position response profiles as '*edge-only*' '*surface*' and '*surface + EE*' (surface with edge enhancement). '*Weak* or *none*' denotes a group of cells that were not activated sufficiently to be classified (although responsive to contrast-defined figures). '*Unclear*' means that the cell was activated, but the position response profile was either flat or not clearly related to surface or edges of the figure. See Section 3 for classification criteria. Edge-only cells make the location and orientation of the edges explicit, which is thought to be essential for stereoscopic shape perception.

the responses to the center. The distribution of the SER differed significantly between V1 and V2, with medians of 0.62 and 0.32, respectively (Kruskal–Wallis, $P < 0.01$, $n_1 = 24$, $n_2 = 31$). The difference was also significant when the unclear cases were included ($P < 0.01$, $n_1 = 27$, $n_2 = 36$). Note, however, that the test was designed post hoc. The 13 cells with the smallest ratios were all from V2. Choosing as a criterion a ratio below 0.2, that is, edge response at least five times stronger than surface response, we classified 12 cells as 'edge-only' (median SER 0.03). Edge-only cells were found in both animals (ten of 63 V2 cells in # 1, and two of 12 V2 cells in # 2).

Fig. 5 summarizes the results for all cells that were tested with cyclopean figures. Responses were classified as *edge-only* (SER < 0.2), *surface* (SER ≥ 0.5), and surface with edge enhancement, *surface* + EE ($0.2 \leq$ SER < 0.5). Edge-only cells constituted 16% of the total sample of V2, or 33% of the cells that were responsive to random-dot stereograms. Edge enhancement was equally frequent in both areas (10 and 12%). The frequency of 'surface' cells was lower in V2 (13%) than in V1 (24%). In a few cells, the position response profiles were not obviously related to surface or edges (*unclear*, V1: 4%, V2: 7%). Sectors labeled weak or none represent the cells that did not respond well to random-dot stereograms (V1: 62%, V2: 52%). Although we cannot not exclude the possibility that a small percentage of edge-only cells also exist in V1, Figs. 4 and 5 suggest that the complete absence of surface responses in random-dot stereograms is a new feature that emerges in V2. While the exact criterion for the definition for 'edge-only' responses is arbitrary, our choice seems to make a meaningful distinction, since the cells thus defined turned out to be also the cells that are orientation selective for cyclopean edges.

3.2. Orientation of contour

Fig. 6 shows the orientation tuning characteristics of two V2-cells for contrast-defined and cyclopean edges. Edge orientation was varied over 360° and responses are plotted as a function of the orientation of the edge normal. Cell 2 has a bimodal tuning, responding about equally to edges of 180° orientation difference (see the corresponding position response profile in Fig. 2). Cell 5 has a monomodal tuning, and this cell responded only to one edge in the position test (cf. cells 3–4 of Fig. 2). In each case, the orientation tunings for contrast border and stereoscopic edge are remarkably similar. The orientation tuning for cyclopean edges was recorded in 16 cells, eight edge-only cells, and eight

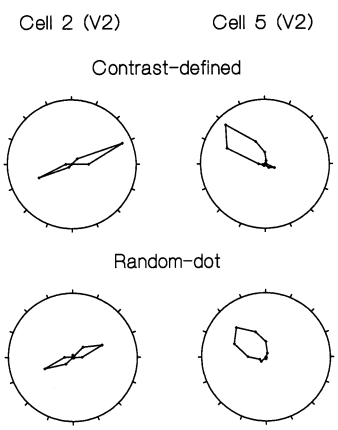

Fig. 6. Orientation tuning for edges of contrast-defined and cyclopean figures in two cells of area V2. The figures were rotated about one of their edges which was centered in the receptive field, and presented at 16 different orientations covering 360°. Mean firing rates are plotted radially against the orientation of the edge normal. Calibration: radius of *circle*, 30 spikes/s, except for cell 2, contrast defined, 60 spikes/s. Despite the stimuli being radically different (see Fig. 1), the cells signaled orientation with equal selectivity. Cell 2: see Fig. 2; cell 5: figure disparity $-7'$, surround disparity 0.

surface cells. Of the edge-only cells, seven were selective for the orientation of cyclopean edges, and the preferred orientation closely matched those for moving contrast bars (range of differences -13 to $+13°$, mean 2.7°, S.D. 9.2°); one showed flat tuning. The surface cells showed either flat tuning ($n = 3$) or erratic tuning curves ($n = 5$). Using the same definition of peak orientation (midpoint at half amplitude of the smoothed tuning curve) the orientation differences ranged from $-31°$ to 84°, with a minimum of 20°.

3.3. Localization of contour

Edge-only cells signaled the position of cyclopean edges accurately, except that the response maxima tended to be displaced towards the center of the figure (range -0.1 to 0.8°, median 0.30°, 18 edge responses in 12 cells). Such a displacement would be expected if the receptive fields had a central summation area for the preferred disparity of about 0.6° width (twice the median displacement). There was a similar but smaller error for contrast-defined figures, so that the median displacement between the stereoscopic and contrast conditions was only 0.10°.

We conclude that edge-only cells represent the location and orientation of contours, whether defined by contrast or by disparity. Cells that were activated by the surface of a cyclopean figure were generally not orientation sensitive when tested with an edge of that figure, despite their orientation selectivity for contrast borders.

3.4. Foreground and background

An interesting observation is that cells 3 and 4 responded only to one of the opposite edges of the squares (Fig. 2). Cell 5 also responded to only one side, as indicated by the single lobe in the 360° orientation tuning curve (Fig. 6). Responses of these cells confer information not only about the location and orientation of edges, but also the direction of the step in depth. For example, a response of cell 3 indicates that the foreground surface extends to the right of its receptive field, while a response of cell 4 indicates that the foreground surface extends to the left. Most (9/12) of the cyclopean edge selective cells showed this asymmetry.

Edge-only cells generally preferred negative (near) disparities: six were 'near cells', four were 'tuned-excitatory' with peaks at -14, -8, -7 and $+1$ arc min, and two cells had flat tuning. Four of the edge-only cells responded exclusively to binocular stimulation. The preference for negative disparities is interesting regarding a possible role in image segmentation and the representation of occluding contours. Occluding contours belong to a foreground object and thus tend to have 'near' disparity.

3.5. Mechanisms in stereoscopic edge detection

While modeling cyclopean edge selectivity is beyond the scope of this paper, the following results throw some light on the mechanisms involved. The lack of responses to the surface of cyclopean figures suggests that the optimal disparity has excitatory as well as inhibitory effects in these cells. Thus, analyzing the interaction of disparities in the receptive field might help to understand the mechanism. Figs. 7 and 8 show results of experiments in which we have independently varied the disparities of figure and surround. We have obtained data of this sort in five cells so far. They illustrate the response suppression that occurs when the local disparities approach the same value, and also demonstrate the observation that edge selective cells are unresponsive to frontoparallel surfaces at any disparity.

An edge of the square figure was centered in the receptive field so that half of the field was stimulated with the figure disparity, the other half with the surround disparity. Fig. 7 shows examples of three cells from V2. Cell 2 was 'tuned-excitatory', cell 4 'near', cell 6 'far', according to moving bar responses (tuning curves at top of figure). According to position response profiles obtained with cyclopean figures, cells 2 and 4 were classified as 'edge-only', cell 6 'surface with edge enhancement'. Cells 4 and 6 responded preferentially to one side of the cyclopean figure (see Fig. 2). The bottom half of Fig. 7 shows the interactions of figure and surround. The axes represent figure and surround disparities, and the size of disks represents the strength of responses. Standard random-dot stereograms (10% density, white/gray) were used for cells 2 and 6. For cell 4, color contrast was added in this test (50% red/gray in figure vs 50% white/gray in surround) because this cell was strongly color selective. The addition of color contrast resulted in responses of 14 spikes/s, compared to only three spikes/s obtained with the cyclopean edge (red/gray dots in figure *and* surround, as shown in Fig. 2).

Comparing these interaction plots with the disparity tuning curves shown at the top one can see that the figure disparity had similar effects in the mean: cell 2 shows activity limited to the vertical column for zero figure disparity, cell 4 shows activity mainly for negative (near) figure disparities, and cell 6 mainly for positive (far) figure disparities. However, the responses are strongly modulated by the disparity on the surround side: cell 2 responds only when the surround disparity is positive (far); cell 4 only when the surround disparity is near zero; cell 6 only when the surround disparity is either lower or higher than the figure disparity. Thus, cyclopean edge selective cells might be conceived as combining the signals of regular 'tuned', 'near', and 'far' cells from either side of the figure boundary. If the cells were combining these signals in

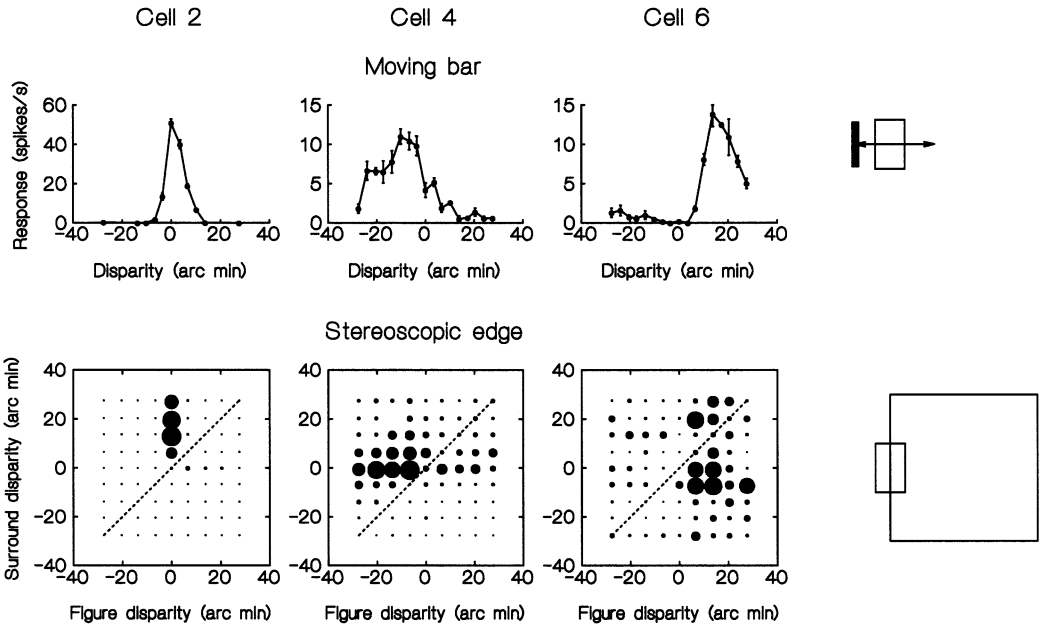

Fig. 7. Interaction of figure and surround disparity in stereoscopic edge responses. Three cells of V2. The top row shows the disparity tunings obtained with contrast-defined moving bars, as shown schematically on the right. The bottom row shows bubble plots of the responses to random-dot stereograms. The edge of a figure was centered in the receptive field, as shown on the right, and figure and surround disparities were varied in factorial manner. Each point represents a combination of disparities (negative = near, positive = far). Points on the diagonal represent stimuli with the same disparity in figure and surround (dashed fine), for points to the left of the diagonal, the figure was nearer than the surround, for points to the right, the figure was farther. Size of *circles* represents mean firing rates (maximum: 19, 14 and 4 spikes/s, respectively, minimum: 0 for all three cells).

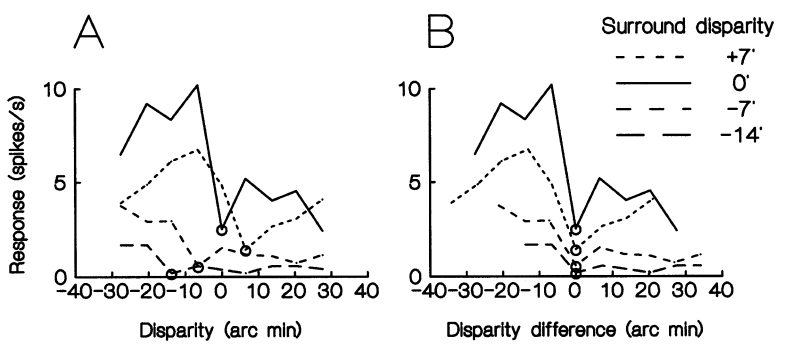

Fig. 8. Stereoscopic edge responses: The effect of varying figure disparity at different levels of surround disparity, as indicated. Data of cell 4 of Fig. 7. In (A) the responses are plotted as a function of figure disparity, in (B) as a function of the difference between figure disparity and surround disparity. The minimum of each curve has been *circled*. In (B) but not in (A) the curves are aligned, indicating that the cell signals disparity difference rather than absolute disparity.

linear fashion the interaction plots would show plaids of horizontal and vertical bands. This was clearly not the case. The plots show clusters of activity, indicating that nonlinear operations are used in combining the disparity signals.

An important feature of the disparity interaction plots of Fig. 7 is the absence of responses on the diagonal, the locus of stimuli in which figure and surround have the same disparity (dashed line). In other words, the cells did not respond to a random-dot plane at any disparity. This was found in all five cells tested. Fig. 8 shows the responses of cell 4 at four levels of surround disparity in more detail. In Fig. 8A, the responses are plotted as a function of the figure disparity, in Fig. 8B, as a function of the difference between figure and surround disparity. Circles mark the minimum of each curve. One can see that the troughs of the curves are aligned when plotted over the disparity difference (Fig. 8B).

3.6. Control for fixation disparity

In interpreting the plots of Fig. 7 we have assumed that the effect of the surround is caused by neural

interaction, and not by changes in the angle of convergence of the eyes. Indeed, if fixation had been dragged by the disparity of the surround, this would have shifted the tuning to figure disparity as a whole; the rows of the interaction plots would then appear similar and stacked along the diagonal. This was clearly not the case. In order to check if the disparate surround changes eye convergence, we recorded the disparity tuning of a sharply tuned cell with and without disparate surround (Fig. 9). In the first case, the fixation target was centered in a blank field of zero disparity, and a small dark bar of varying disparity was moved across the receptive field (solid line). In the other case, the fixation target appeared floating in front of a random-dot background of 14 arc min disparity, and a 2° cyclopean square of varying disparity was centered on the receptive field (dashed curve). It can be seen that the dashed curve is only slightly displaced compared to the solid curve, the midpoint at half height being shifted by 1 arc min. This result demonstrates that the animals are able to maintain precise convergence on the fixation target despite disparate surrounds.

4. Discussion

Our results show that the vast majority of cells of upper-layer V1 and area V2 of the monkey are disparity selective, and about half of the cells can be activated by random-dot stereograms. This is in agreement with previous studies (Poggio et al., 1985; Poggio, Gonzalez & Krause, 1988). However, while the cells of V1 in general respond to stereoscopic surfaces, 33% of the cells of V2 respond exclusively to edges and signal edge orientation. These cells signal the contours of cyclopean and contrast-defined figures consistently. A majority of these cells also signal the step polarity of the contour. Contrarily, cells of upper-layer V1, as well as many cells of V2, signal orientation of contrast-defined contours, but not cyclopean edges. Given the relatively small sample of 69 cells of V1, we cannot exclude the possibility that edge-only cells also exist in area V1, but they are certainly rare. Note also that the assignment to the upper layers of V1 is based on track reconstruction, which has a limited accuracy; it is possible that a few of the V1 cells were actually from layers 4A and 4B.

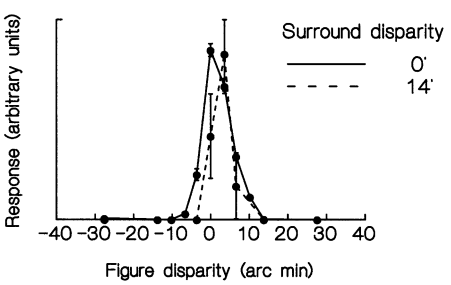

Fig. 9. Control for changes of convergence. Disparity tuning curves of a sharply tuned cell obtained with different background disparities. The monkey was either fixating a target in a blank surround of zero disparity (*solid line*), or a target floating in front of a random-dot surround of 14′ far disparity (*dashed line*). Responses to moving dark bar and cyclopean square, respectively. Responses have been scaled. One can see that there is virtually no displacement between the two curves, indicating that the animal maintained accurate convergence.

Before we discuss stereoscopic edge selectivity further we shall consider possible alternative interpretations of our results. Since natural fixation involves continuous small eye movements, one possibility is that the increased activity for receptive field positions near edges was due to the temporal rather than the spatial pattern of stimulation. The disparity in a receptive field is more likely to vary for receptive field positions close to an edge then in the center of the figure, and some cells might be activated by the variation, but not a constant disparity. The finding of orientation tuning (Fig. 6) and step polarity selectivity (Fig. 2, cells 3 and 4, Fig. 6, cell 5) rules out this explanation. When two opposite edges of the square are positioned in the receptive field, the disparities of the adjacent regions are simply exchanged. Therefore, the statistics of disparity variation produced by random fixational eye movements are similar or identical for the two edges, but only one of them produced a response. Similarly, the temporal variation of disparity would not produce consistent orientation tuning.

Another point to discuss is the role of the alignment of the eyes. Recordings from the awake animal have the advantage that binocular fixation aligns the eyes in the natural manner. However, it does so with some variability. It is difficult to measure the convergence angle with an accuracy of minutes of arc, and we did not attempt such measurements. Could cyclopean edge selectivity (as demonstrated in Fig. 2) be an artifact of varying convergence? The observation is that cells respond to an edge of a plane figure, which has the appropriate disparity, but not to the center of the figure at the same disparity (or any disparity). The only way we can think of to account for this finding in terms of vergence movements is to assume that vergence deviates from its target value when the receptive field under study is in the center of the figure, so as to cancel the figure disparity, but does not deviate when the receptive field is near an edge of the figure. While such behavior might seem unlikely, it could occur in cases where the figure overlaps the fixation point for some positions (resulting in disparity cancellation and no response) but not for other positions (resulting in a response). If the positions at which the figure overlapped the target were roughly the same as the positions at which it overlapped the receptive field, it would appear as if the responses were edge selective, although they were simply disparity selective. First of all, the example of

Fig. 9 shows that disparate random-dot patterns surrounding the fixation target do not generally cause deviations of convergence. Second, we have checked our data for conditions where the figure overlapped target and response field. In the three edge-only cells of Fig. 2, responses to edges and unresponsiveness to surface were both obtained with the fixation target outside the figure. Overall, 12 out of 17 edge responses in the 'edge-only' cells occurred when the figure was far from overlapping the fixation target. Thus, at best, figure-induced convergence changes could explain five out of 17 cases of edge selectivity. Also, 'surface' responses were obtained in many cells even when the figure covered the fixation target; thus, cancellation of disparity did not occur. An example is cell 1 of Fig. 2. Furthermore, if cyclopean edge selectivity were an artifact of vergence movements, it would be extremely unlikely to find similar preferred orientation for the cyclopean edges as for contrast borders (Fig. 6), but the preferred orientations were very similar in every cell in which orientation tuning was found (the standard deviation of the difference was 9.2°). Finally, the different frequency of cyclopean edge selective cells in areas V1 and V2 could not be explained by the eye movement hypothesis. Thus, artifacts of eye movements can be ruled out as explanations of cyclopean edge selectivity.

We have defined cyclopean edge selectivity by the relative strengths of surface and edge responses. A ratio of 0.2 was chosen as a criterion (edge response five times stronger than surface response), which is arbitrary. It seems to capture the essential feature well though, since seven out of eight cells that met this criterion also showed orientation tuning for cyclopean edges that was consistent with the tuning for contrast borders, whereas none of the other eight cells tested did. The lack of orientation selectivity suggests that edge enhancement, which was found in both V1 and V2, is produced by concentric center-surround antagonism (analogous to the center-surround antagonism of retinal ganglion cells for luminance), while complete edge selectivity would result from oriented field structures (perhaps analogous to those of simple cells).

The representation of stereoscopic edges is an example of the known strategy of cortical processing. In the retina, images are encoded in a pointwise fashion by the activity of cells with small, circular receptive fields. In the cortex, this information is transformed into a representation of oriented features (Hubel & Wiesel, 1968). This transformation seems to be fundamental to form perception. The responses to random-dot stereograms in V2 indicate that the cortex follows the same strategy for binocular shape perception. However, this requires an extra step of processing because the images in the two eyes have to be compared and unified before operations that reveal edges can be applied. This hypothetical stage of binocular unification has been called the cyclopean retina (Julesz, 1971). Our findings indicate that the operations for stereoscopic edge detection are first completed in cells of area V2; that is where we find the first signals that make position and orientation of these edges explicit. These cells may therefore be considered as the stereoscopic analogue of V1 simple cells: as simple cells operate on signals originating in the retina, the stereoscopic cells of V2 operate on the output signals of V1. In this view, V1 is Julesz' hypothetical cyclopean retina, the site of the binocular image representation that underlies stereopsis (Julesz, 1971), and V2 the 'cyclopean cortex', which encodes the contours for stereoscopic shape perception.

By 'representation of stereoscopic edges' we refer to the position, orientation, and foreground/background selectivity demonstrated in Figs. 2 and 6. These results mean that, in a world of plane frontoparallel surfaces, the activity of those cells explicitly represents the edges, whether defined by contrast or by disparity. By 'explicitly' we mean that the location and orientation of the edges can be obtained from the activity of that population of cells without much further processing (for example, by using a threshold for firing rate and determining the clusters of active cells in the (position, orientation) parameter space). We do not imply that edges are the optimal stimuli for those cells of V2. Since, in the luminance domain, most V1 cells respond better to sinusoidal gratings of the optimal spatial frequency than to edges (Albrecht, De Valois & Thorell, 1980) it is possible that corrugated stereoscopic surfaces would produce greater responses than stereoscopic edges. Sinusoidal contrast gratings and the tools of linear systems analysis have been used in several studies in order to provide a general functional description of cortical receptive fields. For a linear system, the response to any pattern can be calculated from the responses to sinusoidal gratings. By analogy, one might argue that the use of sinusoidal disparity gratings, would also provide more general information about the stereoscopic properties of neurons. We have not used this approach here because we wanted to provide neurophysiological data for direct comparison with the large body of knowledge from psychophysical studies on cyclopean form perception which used stereograms of plane figures (see Julesz, 1971 for references). In the presence of nonlinearities, calculating the responses to plane squares from the sinusoidal grating responses would be faulty, whereas recording the responses to stereoscopic squares gives an accurate picture of the cortical representation of stereoscopic squares. It might be interesting to determine 'disparity modulation transfer functions' for cells of V1 and V2. Our results suggest that some cells of V2 would show pronounced bandpass tuning, whereas cells of V1 would show mostly low-pass tuning. Note, however, that the asymmetry of the edge responses, which was characteristic of 75% of 'edge-only' cells, could be

shown only by measuring the phase dependence of the grating responses.

Edge selectivity, as displayed by cells 2, 3 and 4 of Fig. 2, is of particular interest because it implies unresponsiveness to frontoparallel surfaces at any disparity. Our experiment in which the disparities on the two sides of an edge were varied independently further illustrates this point, showing that the responses are attenuated whenever the difference between the disparities vanishes, over a range of the common disparity (Figs. 7 and 8). This means that features of 3D objects would evoke relatively constant neural signals even in the presence of variations in object distance, or variations in convergence of the eyes. This feature might be related to the phenomenon in stereopsis that small disparity differences can be discriminated despite variations in absolute disparity (Westheimer & McKee, 1978). It will be important to explore the dependence of neural responses on disparity and disparity difference in the narrow range of about 10 arc min of disparity where this phenomenon is most prominent (Fig. 6 of Westheimer & McKee, 1978).

The issue of relative and absolute disparity has recently been addressed in a study by Cumming and Parker (1999) who tested V1 receptive fields with random-dot stereograms while imposing a disparity by means of feedback-controlled mirrors. Eye-movement feedback served to cancel vergence movements so that the whole stimulus configuration could be presented at a disparity for short periods of time. The results showed that V1 cells in general responded according to the disparity of the stimulus dots in the receptive field and were not influenced by the disparity of a surrounding annulus or by the vergence angle. Our finding of incomplete surface suppression in V1 (Fig. 4) seems to agree with this result in showing that influences from the receptive field surround are generally weak in this area. However, the results of the two studies are not directly comparable since Cumming and Parker (1999) studied receptive fields only in the center of a region of constant disparity, purposely avoiding mixture of disparities in the receptive field, whereas the comparison between edge- and surface responses was the main point of our experiments. Cumming and Parker used artificially controlled fixation disparity, while our experiments were done under natural control of fixation. Thus, we do not know the surface to edge response ratios for the cells of Cumming and Parker's sample, nor do we know if V2 cells would respond according to relative disparity when their receptive fields were placed in the center of a disk/annulus configuration as in Cumming and Parker's experiment.

We do not yet understand the mechanisms of stereoscopic edge selectivity. A differencing of disparity selective signals with the same tuning but spatially offset receptive fields, analogous to the classical simple cell model in the luminance domain, might be the basic underlying operation (Gray, Pouget, Zemel, Nowlan & Sejnowski, 1998). The question whether the input comes from binocular comparators sensing position disparity or phase disparity (Ohzawa, DeAngeles & Freeman, 1996), although interesting in itself, appears irrelevant at this point; both kinds of comparators could presumably be used as the input to such mechanisms. The disparity interaction patterns of Fig. 7 suggest that signals of different tuning types ('tuned excitatory', 'near' and 'far') are combined in stereoscopic edge cells, and that the combination involves nonlinear 'gating' operations. However, the underlying neural mechanisms may be more complex than that. Recent studies of the interaction of disparity and occlusion cues in 3D surface perception have shown that the presence of image elements in one eye that are missing in the other eye plays an important role ('half-occlusion'; Anderson & Nakayama, 1994; Gillam, Blackburn & Nakayama, 1999). Mechanisms that involve half-occlusion and mechanisms that use disparity signals, as sketched above, cannot be disentangled with the present type of random-dot stereograms because these stereograms provide disparity as well as half-occlusion cues.

Studies of perception have demonstrated the sophistication of the mechanisms of cyclopean form perception (Julesz, 1971). Specifically, psychophysical experiments indicated the existence of cells that are orientation selective for cyclopean stimuli (Tyler, 1975; Mustillo, Francis, Oross, Fox & Orban, 1988; Hamstra & Regan, 1995). These studies suggest that human perception uses a representation similar to the one we have demonstrated in monkey visual cortex.

The existence of a cyclopean edge representation does not imply, obviously, that this representation is the 'site of cyclopean form perception'. While we assume that perception cannot use information that is not represented in the nervous system, not all of the information that is represented may be used in perception. For example, V1 cells can be strongly modulated by color flicker although no flicker is perceived (Gur & Snodderly, 1997); other V1 cells are modulated by the disparity of contrast-reversed stereograms although such stereograms do not produce depth perception (Cumming & Parker, 1997). Signals may be used elsewhere in the system (contrast-reversed stereograms can drive vergence movements: Masson, Busettini & Miles, 1997), or may not be used at all.

Binocular disparity has a profound influence on the perception of surface in general and affects various aspects of surface appearance, including color and transparency (Nakayama, Shimojo & Ramachandran, 1990). Thus, it should not come as a surprise to find color and disparity selectivity combined in single cells, as we have observed in some cases. This linkage needs

to be studied more systematically. Stereograms such as that of Fig. 1B create a strong illusion of a figure placed on top of, and occluding, a background surface. Some illusory contour figures also produce this perception of occlusion (Kanizsa, 1955; Coren, 1972; Kanizsa, 1979). The visual system generally tries to interpret 2D images in terms of objects in 3D space. Finding the occluding contours (contours that mark discontinuity of depth) is of primary importance for this task, because these contours separate foreground and background information, and provide clues to the shape of the foreground objects. Our finding of stereoscopic contour representation in area V2 supports the earlier conclusion, derived from experiments with illusory contours, that figure/ground segregation and the elaboration of occluding contours are primary goals of processing in area V2 (von der Heydt, Peterhans & Baumgartner, 1984; von der Heydt, 1994; Baumann, van der Zwan & Peterhans, 1997). While those studies based the argument on relatively subtle perceptual effects produced by pictorial cues, our finding of cells that are selective for the step polarity of stereoscopic edges is direct evidence for the coding of the foreground/background direction of contours.

Acknowledgements

We gratefully acknowledge the use of the experimental setup and software developed by G.F. Poggio. We wish to thank Ofelia Garalde, Hai Dong and Clark Jefcoat for technical assistance, and S.S. Hsiao, E. Niebur, G.F. Poggio, and M.A. Steinmetz for helpful comments on earlier versions the manuscript. This work was supported by research grant EY02966 from the National Eye Institute, and grant RG-31 from the Human Frontier Science Program. H.S.F. was supported by the Whitaker Foundation.

References

Albrecht, D. G., De Valois, R. L., & Thorell, L. G. (1980). Visual cortical neurons: are bars or gratings the optimal stimuli? *Science*, *207*, 88–90.

Anderson, B. L., & Nakayama, K. (1994). Toward a general theory of stereopsis: binocular matching, occluding contours, and fusion. *Psychological Review*, *101*, 414–445.

Barlow, H. B., Blakemore, C., & Pettigrew, L. D. (1967). The neural mechanism of binocular depth discrimination. *Journal of Physiology* (*London*), *193*, 327–342.

Baumann, R., van der Zwan, R., & Peterhans, E. (1997). Figure-ground segregation at contours: a neural mechanism in the visual cortex of the alert monkey. *European Journal of Neuroscience*, *9*, 1290–1303.

Coren, S. (1972). Subjective contours and apparent depth. *Psychological Review*, *79*, 359–367.

Cumming, B. G., & Parker, A. J. (1997). Responses of primary visual cortical neurons to binocular disparity without depth perception. *Nature*, *389*, 280–283.

Cumming, B. G., & Parker, A. J. (1999). Binocular neurons in V1 of awake monkeys are selective for absolute, not relative, disparity. *Journal of Neuroscience*, *19*, 5602–5618.

Gillam, B., Blackburn, S., & Nakayama, K. (1999). Stereopsis based on monocular gaps: metrical encoding of depth and slant without matching contours. *Vision Research*, *39*, 493–502.

Gray, M., Pouget, A., Zemel, R., Nowlan, S., & Sejnowski, T. (1998). Reliable disparity estimation through selective integration. *Visual Neuroscience*, *15*, 511–528.

Gur, M., & Snodderly, D. M. (1997). A dissociation between brain activity and perception: chromatically opponent cortical neurons signal chromatic flicker that is not perceived. *Vision Research*, *37*, 377–382.

Hamstra, S., & Regan, D. (1995). Orientation discrimination in cyclopean vision. *Vision Research*, *35*, 365–374.

Hubel, D. H., & Wiesel, T. N. (1968). Receptive fields and functional architecture of monkey striate cortex. *Journal of Physiology* (*London*), *195*, 215–243.

Hubel, D., & Wiesel, T. (1970). Cells sensitive to binocular depth in area 18 of the macaque monkey cortex. *Nature* (*London*), *225*, 41–42.

Hubel, D. H., & Livingstone, M. S. (1987). Segregation of form, color, and stereopsis in primate area 18. *Journal of Neuroscience*, *7*, 3378–3415.

Julesz, B. (1960). Binocular depth perception of computer-generated patterns. *Bell System Technical Journal*, *39*, 1125–1161.

Julesz, B. (1971). *Foundations of cyclopean perception*. Chicago: University of Chicago Press.

Kanizsa, G. (1955). Margini quasi-percettivi in campi con stimulazione omogenea. *Rivista di psicologia*, *49*, 7–30.

Kanizsa, G. (1979). *Organization in vision. Essays on Gestalt perception*. New York: Praeger.

Masson, G. S., Busettini, C., & Miles, F. A. (1997). Vergence eye movements in response to binocular disparity without depth perception. *Nature*, *389*, 283–286.

Mustillo, P., Francis, E., Oross, S., Fox, R., & Orban, G. (1988). Anisotropies in global stereoscopic orientation discrimination. *Vision Research*, *28*, 1315–1321.

Nakayama, K., Shimojo, S., & Ramachandran, V. S. (1990). Transparency: relation to depth, subjective contours, luminance and neon color spreading. *Perception*, *19*, 497–513.

Nikara, T., Bishop, P., & Pettigrew, J. (1968). Analysis of retinal correspondence by studying receptive fields of binocular single units in cat striate cortex. *Experimental Brain Research*, *6*, 353–372.

Ohzawa, L., DeAngeles, G. C., & Freeman, R. D. (1996). Encoding of binocular disparity by simple cells in the cat's visual cortex. *Journal of Neurophysiology*, *75*, 1779–1805.

Poggio, G. F., & Fischer, B. (1977). Binocular interaction and depth sensitivity in striate and prestriate cortex of behaving rhesus monkey. *Journal of Neurophysiology*, *40*, 1392–1405.

Poggio, G. F., Motter, B. C., Squatrito, S., & Trotter, Y. (1985). Responses of neurons in visual cortex (V1 and V2) of the alert macaque to dynamic random-dot stereograms. *Vision Research*, *25*, 397–406.

Poggio, G. F., Gonzalez, F., & Krause, F. (1988). Stereoscopic mechanisms in monkey visual cortex: binocular correlation and disparity selectivity. *Journal of Neuroscience*, *8*, 4531–4550.

Poggio, G. F. (1995). Mechanisms of stereopsis in monkey visual cortex. *Cerebral Cortex*, *3*, 193–204.

Tyler, C. W. (1975). Stereoscopic tilt and size aftereffects. *Perception*, *4*, 187–192.

von der Heydt, R. (1994). Form analysis in visual cortex. In M. S. Gazzaniga, *The cognitive neurosciences* (pp. 365–382). Cambridge, MA: MIT Press.

von der Heydt, R., & Peterhans, E. (1989). Mechanisms of contour perception in monkey visual cortex. 1. Lines of pattern discontinuity. *Journal of Neuroscience*, *9*, 1731–1748.

von der Heydt, R., Peterhans, E., & Baumgartner, G. (1984). Illusory contours and cortical neuron responses. *Science*, *224*, 1260–1262.

von der Heydt, R., Zhou, H., & Friedman, H. (1995). Neurons of area V2 of visual cortex detect cyclopean edges. *Perception*, *24*, supplement 6.

Westheimer, G., & McKee, S. P. (1978). Stereoscopic acuity for moving retinal images. *Journal of the Optical Society of America*, *68*, 450–455.